

Supporting Information

Heteroepitaxy of GaP on Silicon for Efficient and Cost-Effective Photoelectrochemical Water Splitting

Mahdi Alqahtani^{1,2}, Sanjayan Sathasivam³, Fan Cui¹, Ludmilla Steier⁴, Xueming Xia³, Chris Blackman³, Eunsoo Kim⁵, Hyunjung Shin⁶, Mourad Benamara⁶, Yuriy I. Mazur⁶, Gregory J. Salamo⁶, Ivan P. Parkin³, Huiyun Liu¹, and Jiang Wu^{1,7*}*

¹Department of Electronic and Electrical Engineering, University College London, London WC1E 7JE, United Kingdom.

²King Abdulaziz City for Science and Technology (KACST), Riyadh 12371, Saudi Arabia

³Department of Chemistry, University College London, London WC1H 0AJ, United Kingdom

⁴Department of Chemistry, Imperial College London, London SW7 2AZ, United Kingdom

⁵Department of Energy Science, Sungkyunkwan University, Seoul 440-746 South Korea

⁶Institute for Nanoscience and Engineering, University of Arkansas, Fayetteville, AR 72701, USA

⁷Institute of Fundamental and Frontier Sciences, University of Electronic Science and Technology of China, Chengdu 610054, China

Table of Contents

Supplementary Information Figure S1. Atomic Force Microscopy (AFM) images of the GaP thin film directly grown on a Si substrate.

Supplementary Information Figure S2. AFM surface topography and bright field TEM image for the Si/GaP structure, showing a small number of threading dislocation, terminating at the surface.

Supplementary Information Figure S3. Fitting of the photoluminescence spectrum of the Si/GaP film.

Supplementary Information Figure S4. The cross-sectional STEM images of the Si/GaP-TiO₂-Pt structure at different magnifications.

Supplementary Information Figure S5. STEM EDS line profiling of the Si/GaP-TiO₂-Pt structure.

Supplementary Information Figure S6. The cross-sectional STEM images of the Si/GaP-TiO₂-MoS₂ structure at different magnifications.

Supplementary Information Figure S7. STEM EDS line profiling of the Si/GaP-TiO₂-MoS₂ structure.

Supplementary Information Figure S8. H₂ production for a gas-tight 3-electrode photoelectrochemical cell using the Si/GaP-TiO₂-Pt photoelectrode.

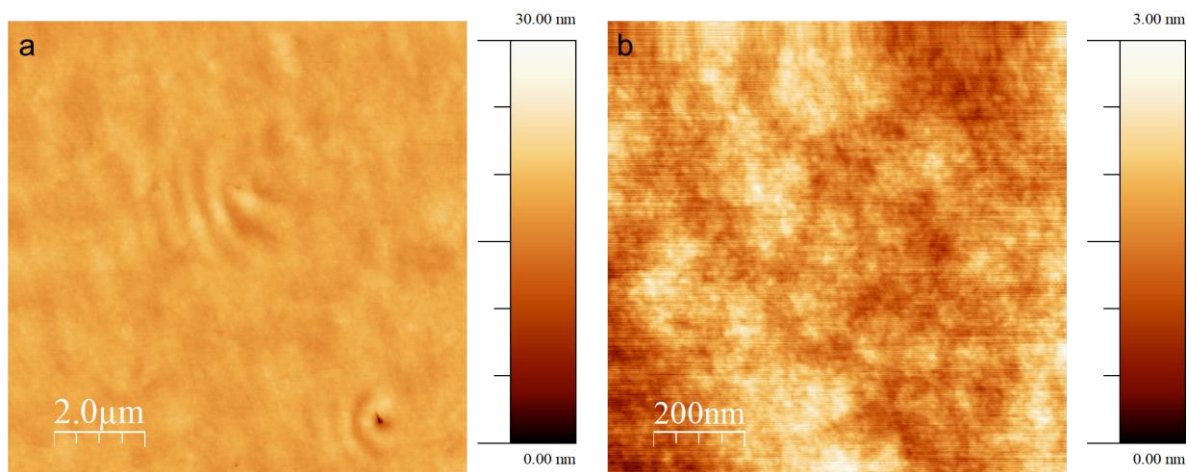
Supplementary Information Figure S9. H₂ production for a gas-tight 3-electrode photoelectrochemical cell using the GaP-TiO₂-Pt photoelectrode.

Supplementary Information Figure S10. Faradaic efficiency measurements for H₂ production.

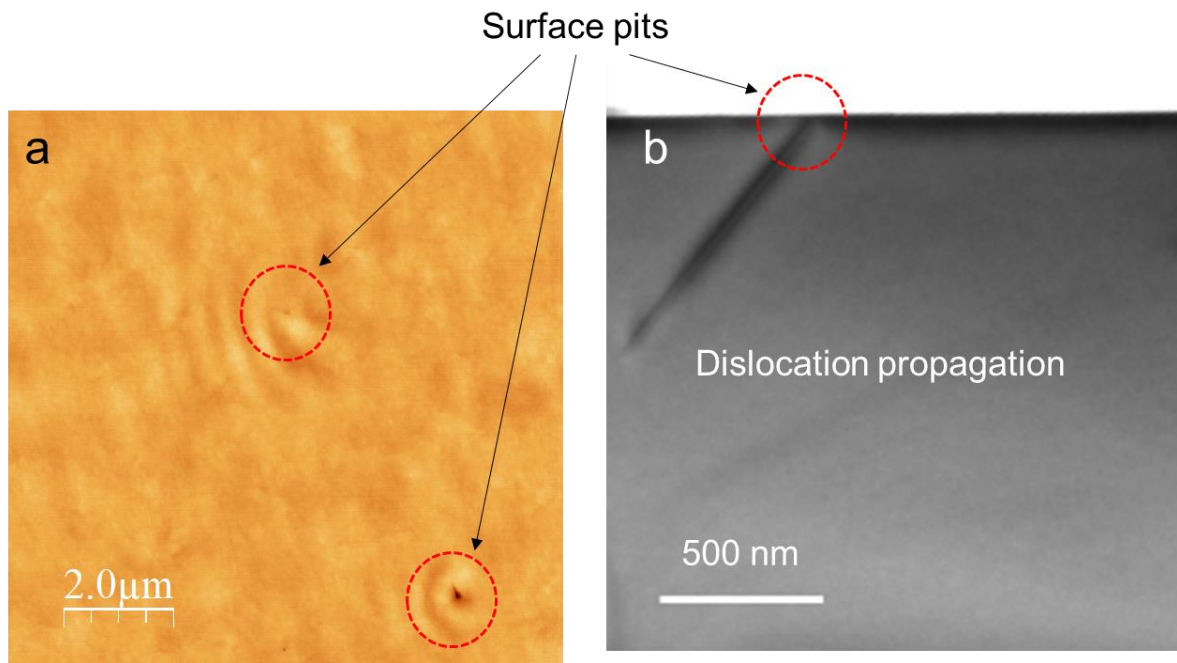
Supplementary Information Figure S11. The experimental setup used for the photoelectrochemical measurements.

Supplementary Information Figure S12. Magnified SEM images of the photocathode surface after reliability test.

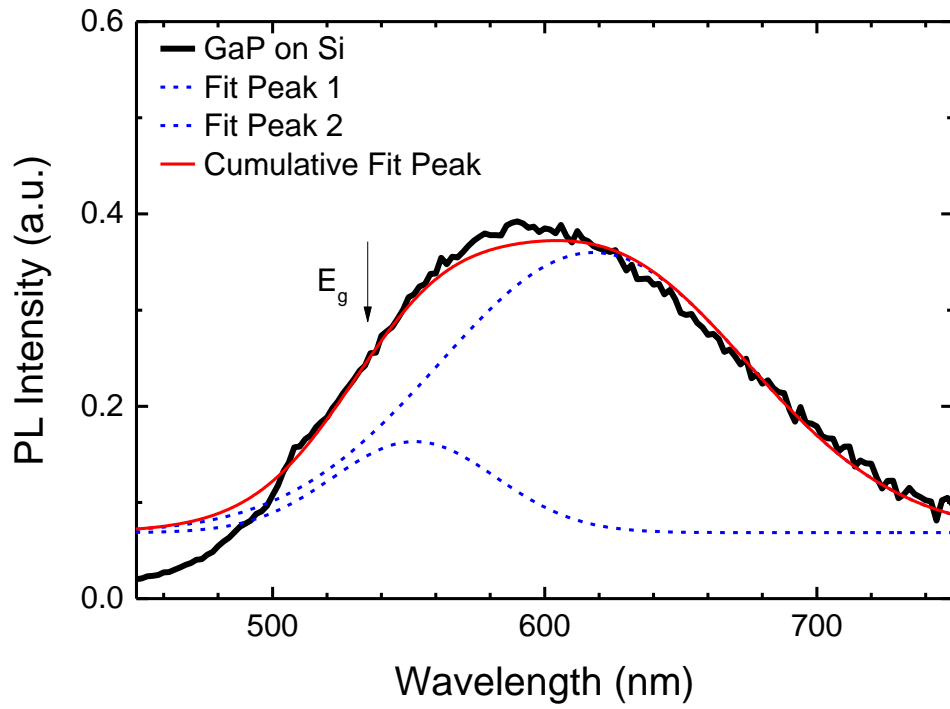
Supplementary Information Figure S13. AFM surface morphology the photoelectrodes after reliability test.



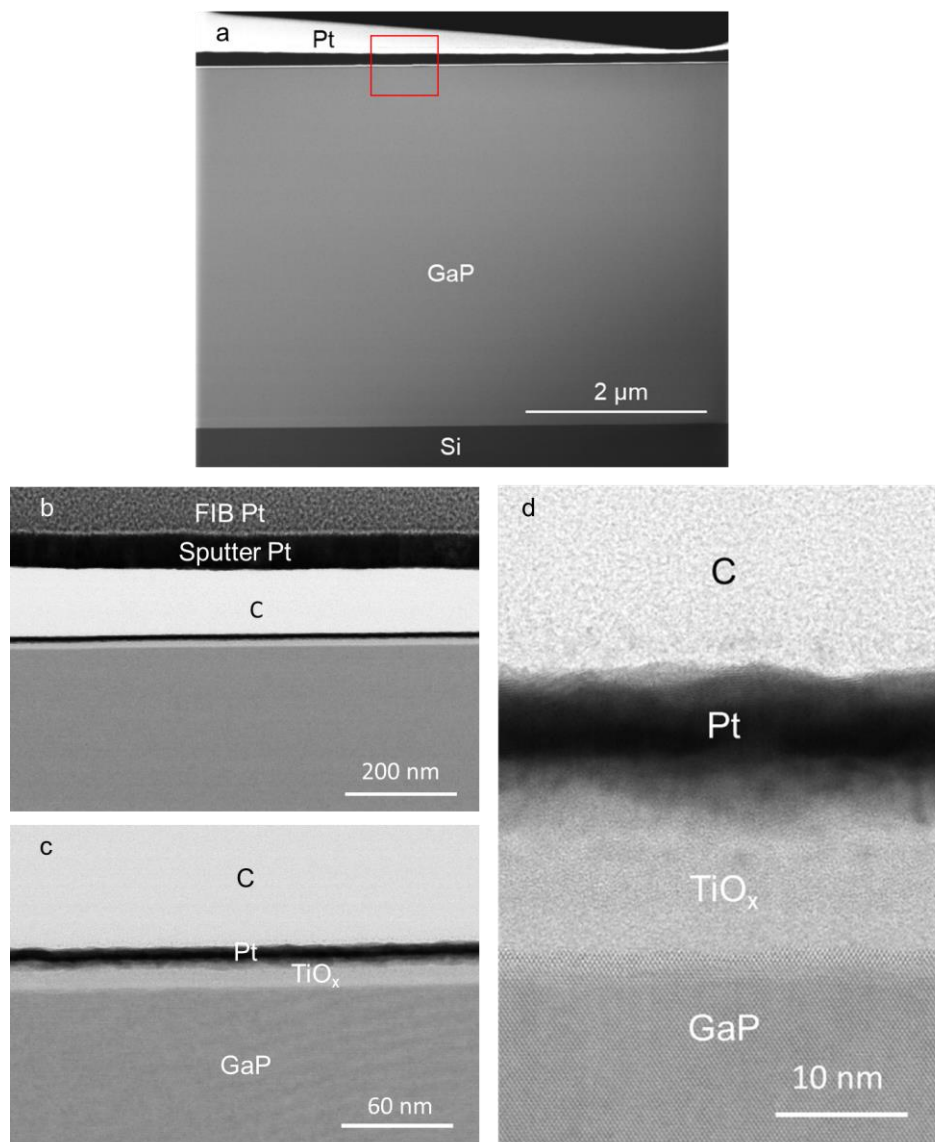
Supplementary Information Figure S1. Atomic Force Microscopy (AFM) images of the GaP thin film directly grown on a Si substrate: **a.** $10 \times 10 \mu\text{m}^2$ and **b.** $1 \times 1 \mu\text{m}^2$. The z-scale is 30 nm and 3 nm for the AFM images in (a) and (b) respectively. The root mean square roughness measured from the AFM images in (a) and (b) are 0.8 nm and 0.39 nm, respectively.



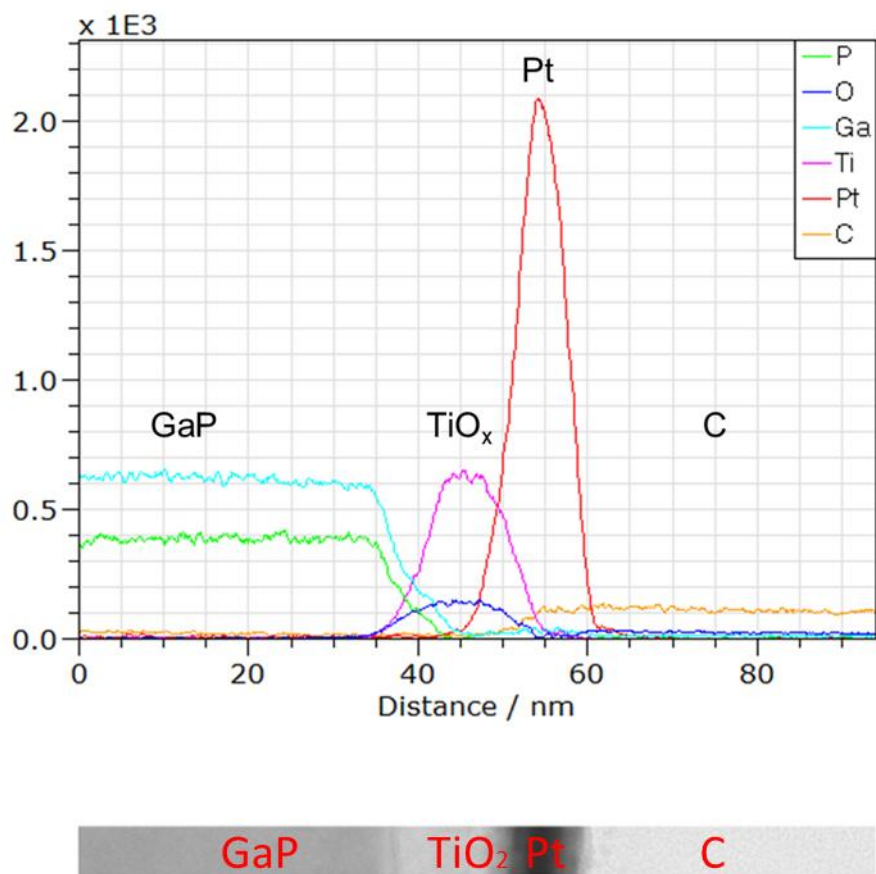
Supplementary Information Figure S2. **a.** AFM surface topography and **b.** bright field TEM image for the Si/GaP structure, showing a small number of threading dislocations terminating at the surface. Most of the dislocations are annihilated in the epilayer, but some of the threading dislocations propagate towards the surface and are terminated at the surface pits. The density of dislocations propagating from the interface is very similar to the density throughout the entire structure. The atomic force microscopy image over the $10\ \mu\text{m} \times 10\ \mu\text{m}$ scan region gives a low density of threading dislocation of the order of $2 \times 10^6\ \text{cm}^{-2}$, which is in agreement with the TEM and XRD measurements.



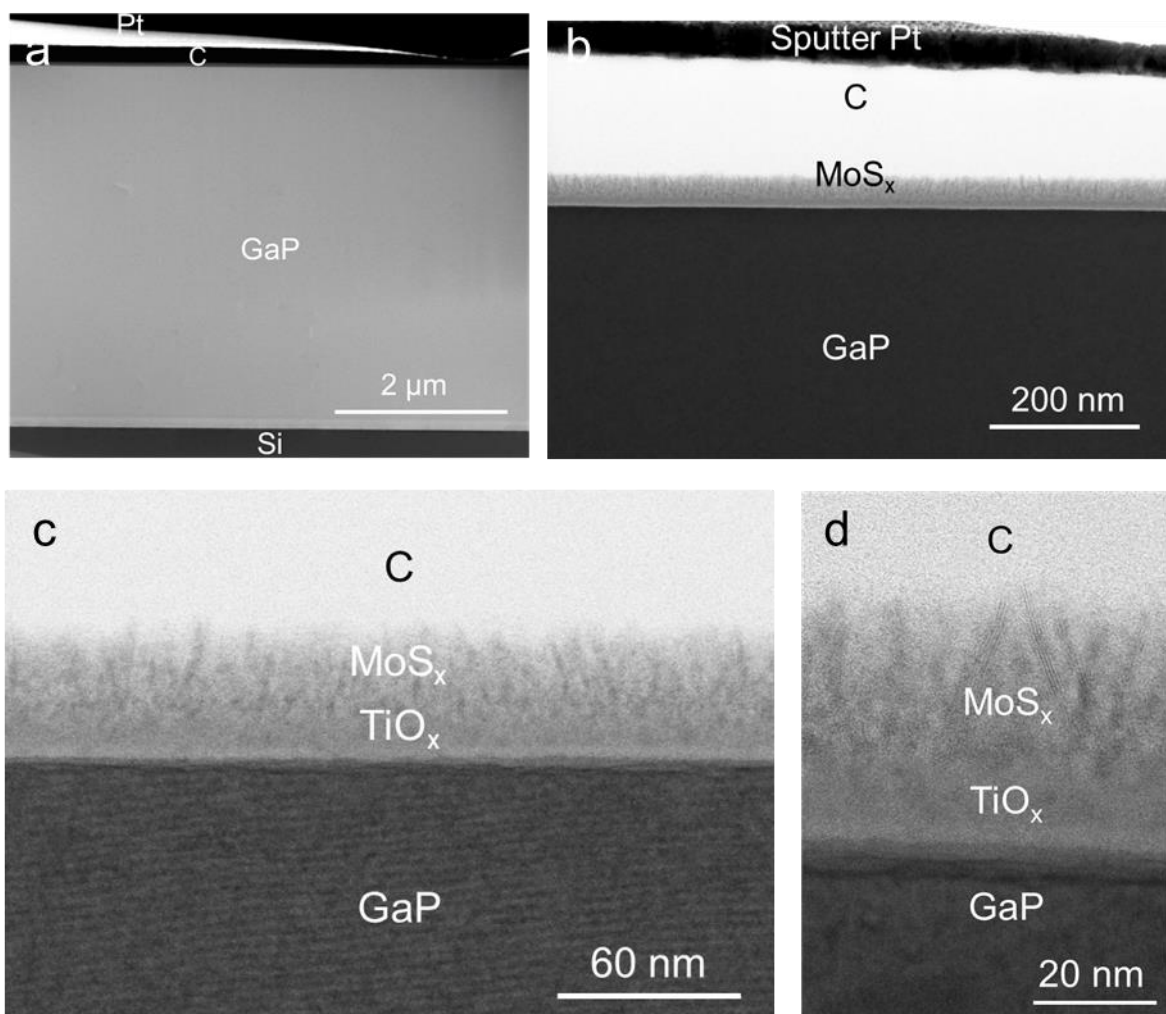
Supplementary Information Figure S3. Fitting of the photoluminescence spectrum of the Si/GaP film. The peak 1 at around 550 nm corresponds to the bandgap of GaP.



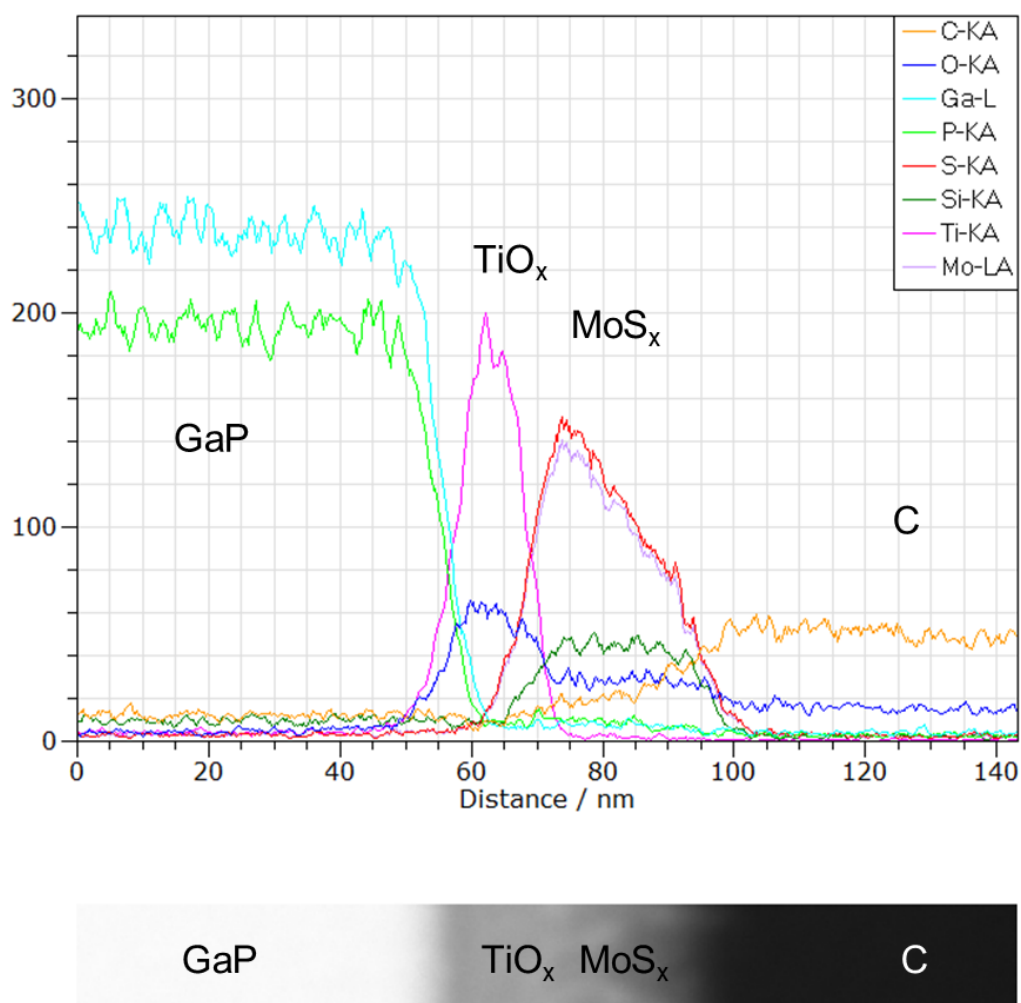
Supplementary Information Figure S4. **a.** The cross-sectional TEM images of the entire Si/GaP-TiO₂-Pt structure. **(b-d).** Transmitted electron STEM images of the ALD deposited TiO₂ protective layer and Pt catalyst layer at different magnifications. FIB Pt, sputtered Pt and C are from sample preparation. C and/or Pt protective coatings were applied prior to FIB milling.



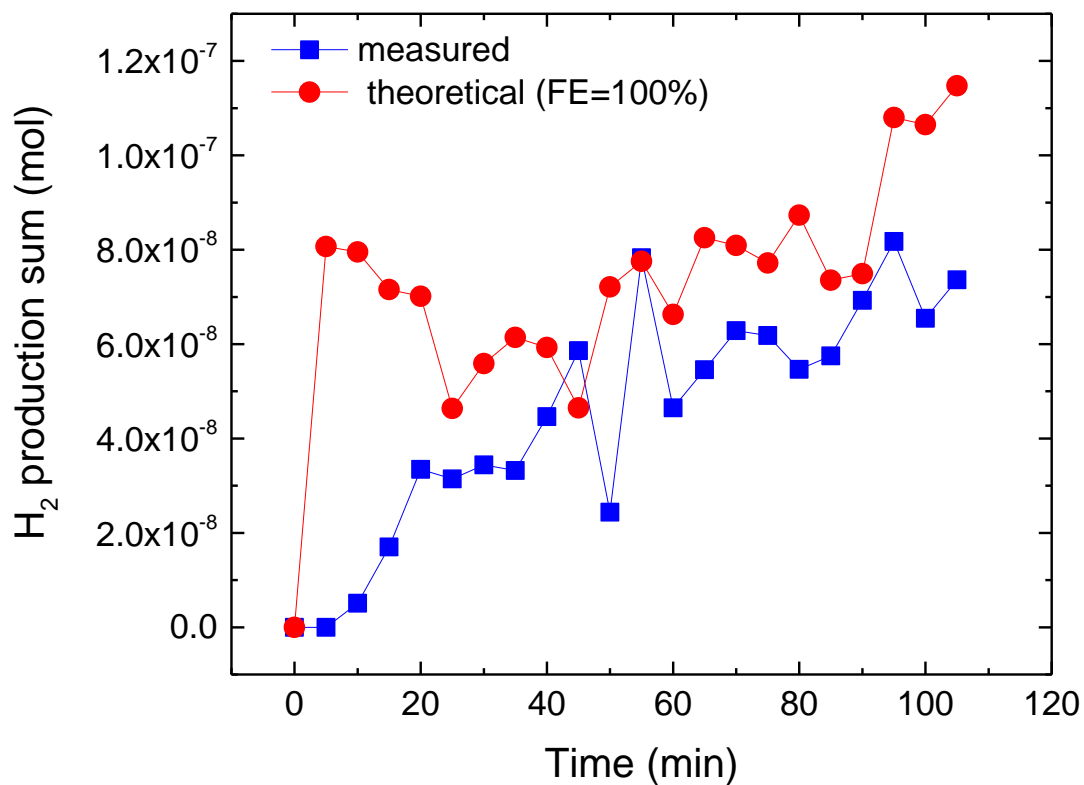
Supplementary Information Figure S5. STEM EDS line profiling coupled with spectral component matching showing the individual layer thickness for TiO_x and Pt. The Y-axis is un-calibrated element intensity. Note that there is some inter-diffusion in the GaP/TiO_x interface and TiO_x/Pt interface. The inset is the STEM image where the EDS line profiling was taken.



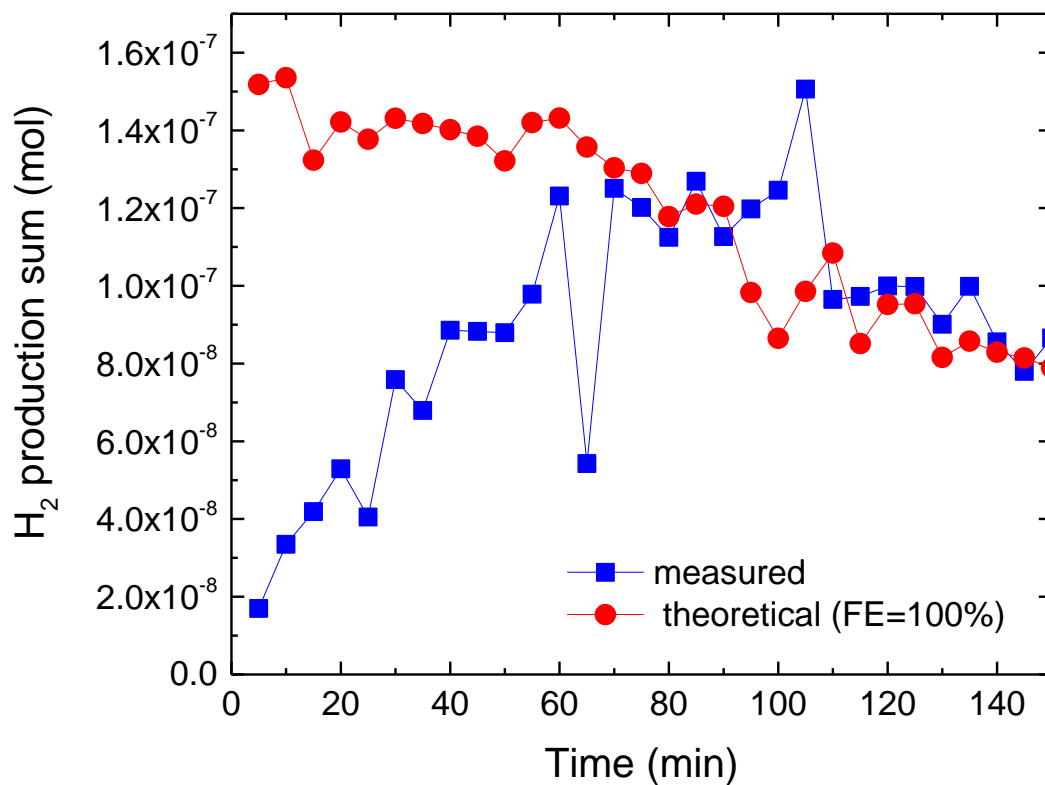
Supplementary Information Figure S6. **a.** The cross-sectional high-angle annular dark-field (HAADF) STEM images of the entire Si/GaP-TiO₂-MoS₂ structure. **b-d.** Transmitted electron STEM images of the ALD deposited TiO₂ protective layer and MoS₂ catalyst layer at different magnifications. Sputtered Pt and C are from sample preparation. C and/or Pt protective coatings were applied prior to FIB milling.



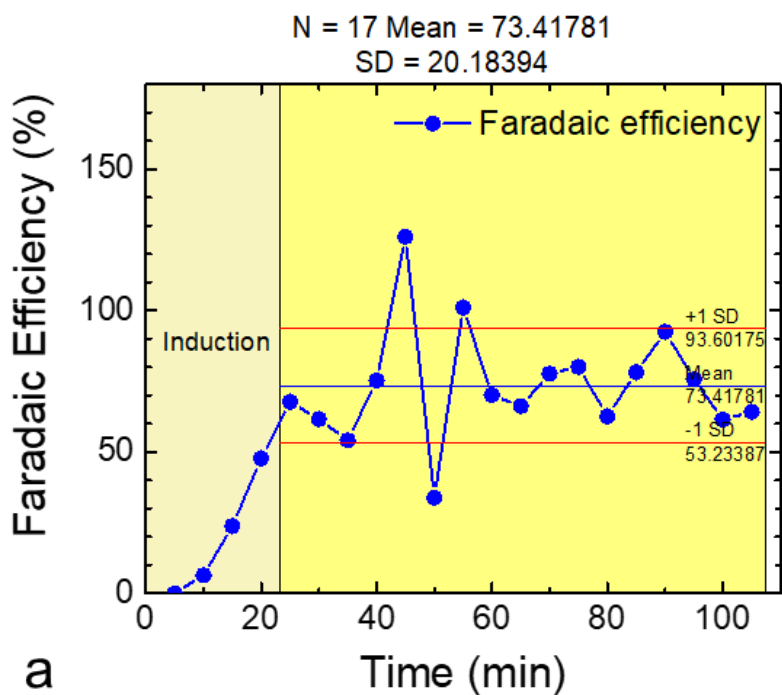
Supplementary Information Figure S7. STEM EDS line profiling coupled with spectral component matching showing the individual layer thickness for TiO_x and MoS_x. The Y-axis is un-calibrated element intensity. The inset is the STEM image where the EDS line profiling was taken.



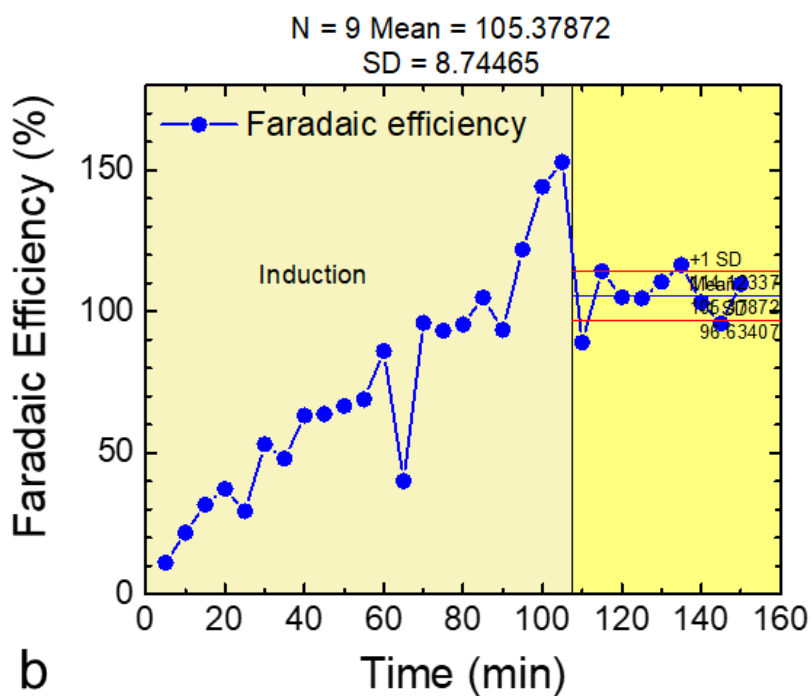
Supplementary Information Figure S8. H₂ production measured with a Clark H₂ sensor in a gas-tight 3-electrode photoelectrochemical cell under illumination and a constant potential at -0.39 V vs. RHE. The photocathode is the the Si/GaP-TiO₂-MoS₂ photoelectrode. The red dots indicate the calculated H₂ production by assuming Faradaic efficiency of 100%.



Supplementary Information Figure S9. H₂ production measured with a Clark H₂ sensor in a gas-tight 3-electrode photoelectrochemical cell under illumination and constant potential at -0.09 V vs. RHE. The photocathode is the GaP-TiO₂-Pt photoelectrode. The red dots indicate the calculated H₂ production by assuming Faradaic efficiency of 100%.



a

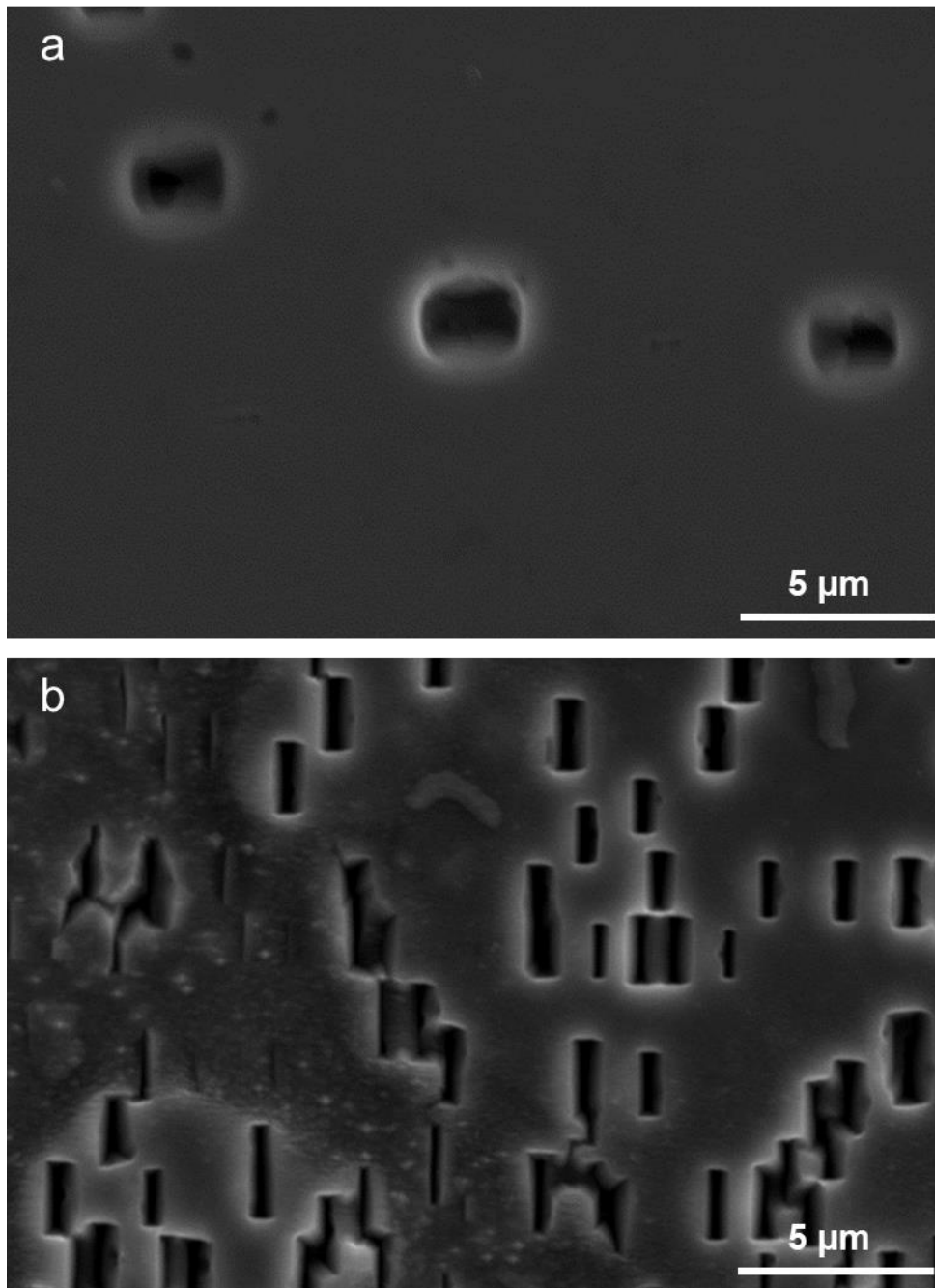


b

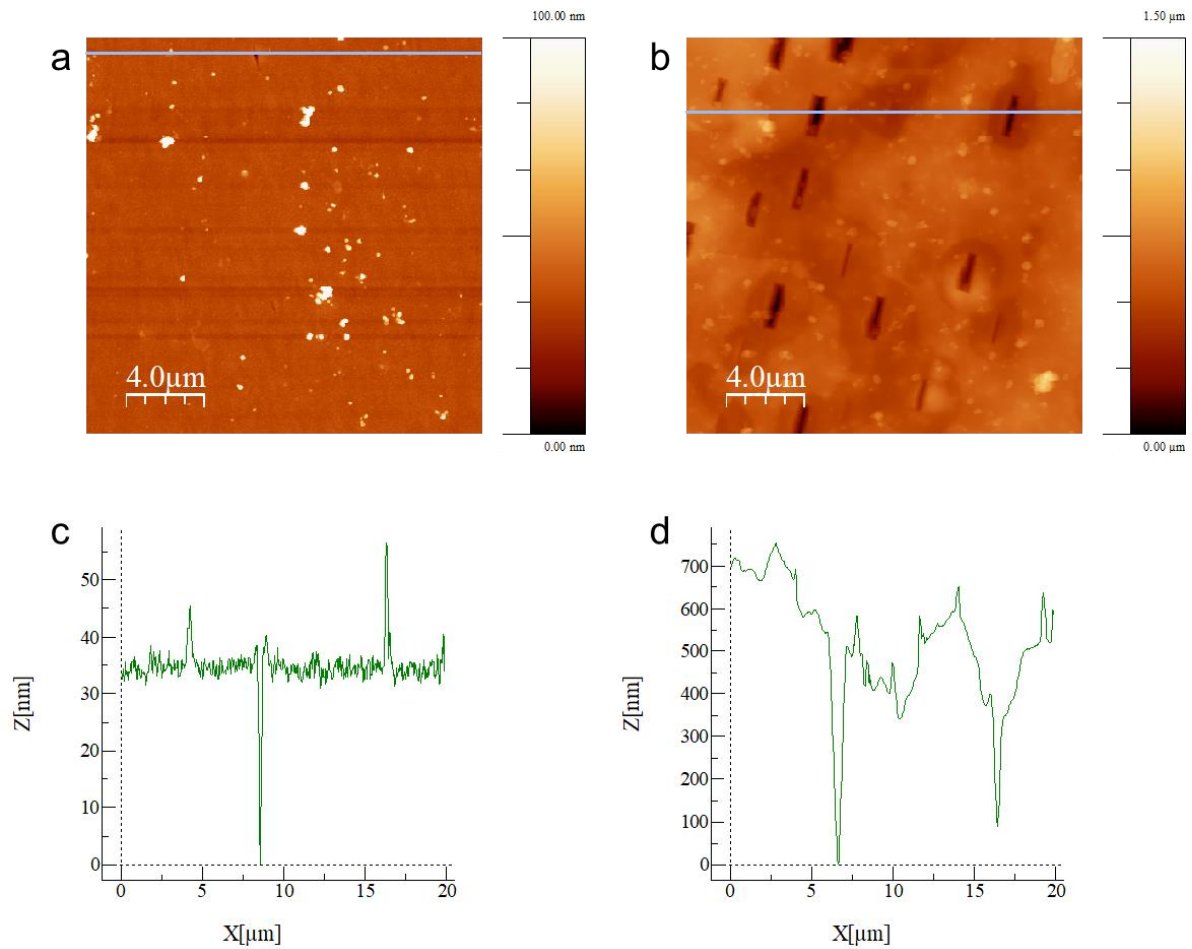
Supplementary Information Figure S10. Faradaic efficiency of H₂ production measured with a Clark H₂ sensor in a gas-tight 3-electrode photoelectrochemical cell under illumination and constant potential. a) FE of the Si/GaP-TiO₂-MoS₂ photoelectrode held at -0.39 V vs. RHE. b) FE of the GaP-TiO₂-Pt photoelectrode held at -0.09 V vs. RHE.



Supplementary Information Figure S11. The experimental setup used for the photoelectrochemical measurements which consists of the working electrode, GaP, Ag/AgCl (sat'd KCl) reference electrode, and a Pt mesh counter electrode immersed in 0.1 M H₂SO₄ (pH 1.1).



Supplementary Information Figure S12. Magnified SEM images of the surface for **a.** Si/GaP-TiO₂-MoS₂ and **b.** Si/GaP-TiO₂-Pt after reliability test (> 3h).



Supplementary Information Figure S13. $20\ \mu\text{m} \times 20\ \mu\text{m}$ AFM surface morphology the photoelectrodes after reliability test ($> 3\text{h}$): **a.** Si/GaP-TiO₂-MoS₂ and **b.** Si/GaP-TiO₂-Pt. AFM line profile of the photoelectrode surfaces after reliability test: **c.** Si/GaP-TiO₂-MoS₂ and **d.** Si/GaP-TiO₂-Pt. The RMS roughness measured from **a.** is 7.8 nm while from **b.** 97.2 nm. The depth of etching pits on the Si/GaP-TiO₂-MoS₂ photocathode is about 30 nm. In contrast, the pits are as deep as 500 nm on the Si/GaP-TiO₂-Pt surface.